A large-scale ^{19}F MRI-based cell migration assay to optimize cell therapy

F. Bonetto[a,b†], M. Srinivas[a], B. Weigelin[c], L. J. Cruz[a], A. Heerschap[b], P. Friedl[c], C. G. Figdor[a] and I. J. M. de Vries[a]*

Adoptive transfer of cells for therapeutic purposes requires efficient and precise delivery to the target organ whilst preserving cell function. Therefore, therapeutically applied cells need to migrate and integrate within their target tissues after delivery, e.g. dendritic cells (DCs) need to migrate to lymph nodes to elicit an antigen-specific immune response. Previous studies have shown that inappropriate cell delivery can hinder DC migration and result in insufficient immune induction. As migration can be extremely difficult to study quantitatively *in vivo*, we propose an *in vitro* assay that reproduces key *in vivo* conditions to optimize cell delivery and migration *in vivo*. Using DC migration along a chemokine gradient, we describe here a novel ^{19}F MR-based, large-scale, quantitative assay to measure cell migration in a three-dimensional collagen scaffold. Unlike conventional migration assays, this set-up is amenable to both large and small cell numbers, as well as opaque tissue samples and the inclusion of chemokines or other factors. We labeled primary human DCs with a ^{19}F label suitable for clinical use; $(0.5-15) \times 10^6$ cells in the scaffolds were imaged sequentially, and migration was assessed using two independent methods. We found no migration with larger numbers of cells, but up to 3% with less than one million cells. Hence, we show that the cell density in cell bolus injections has a decisive impact on migration, and this may explain the limited migration observed using large cell numbers in the clinic. Copyright © 2012 John Wiley & Sons, Ltd.

Keywords: cell migration; migration assays; dendritic cell immunotherapy; ^{19}F MRI; quantification

INTRODUCTION

Dendritic cells (DCs) possess the distinctive ability to initiate primary immune responses. They originate from bone marrow and are present in an immature state in blood and peripheral tissues (1). DCs become activated, for example by infection, and then mature and migrate to the lymph nodes, where they present antigen to the effector cells of the immune system, such as T cells (2). This vital role of the induction of immune responses forms the basis of immunotherapy to treat cancer patients: autologous DCs are matured and loaded with tumor antigen *ex vivo*, before transfer to the patient, where the DCs can activate T cells in the lymph nodes to recognize and fight the tumor (3–6). However, the success of DC immunotherapy has been limited, as only small numbers of DCs actually reach the lymph nodes in patients. Although recent clinical trials have shown positive results, typically less than 4% of the total injected DCs actually reach the lymph nodes (4,5,7–9). In order to improve the efficacy of DC vaccination, a full optimization process of several technical aspects (preparation of the injection region, cell bolus injection density, frequency of vaccination, etc.) is required (10,11). However, this is not feasible *in vivo*. Hence, to effectively assess the efficiency of vaccination procedures, it is crucial to track and quantify the transplanted cells *in vitro* with a real size scale and in a noninvasive manner. Established cell migration assays, typically based on microscopy or the Transwell system, are restricted to thousands or, at most, tens of thousands of cells (12), and therefore are not comparable with the clinical situation of millions of cells migrating in three dimensions over longer distances.

Several noninvasive imaging methods have been used to track DCs *in vivo* or *in vitro*: bioluminescence imaging (13), positron emission tomography (14,15), planar gamma scintigraphy (7,8,15–17), fluorescence of near-infrared-emitting quantum dots (18,19) and MRI (8,20–23). Among them, MRI has been demonstrated to be one of the most successful techniques in the clinic with exquisite spatial resolution and no use of radioactive labels. Furthermore, MRI has already been applied to clinical cell tracking (8).

* Correspondence to: I. J. de Vries, Department of Tumor Immunology, Radboud University Nijmegen Medical Center, PO Box 9101, 6500 HB Nijmegen, the Netherlands.
  E-mail: J.deVries@ncmls.ru.nl

a F. Bonetto, M. Srinivas, L. J. Cruz, C. G. Figdor, I. J. M. Vries
  Department of Tumor Immunology, Nijmegen Center for Molecular Life Sciences, Radboud University Nijmegen Medical Center, Nijmegen, the Netherlands

b F. Bonetto, A. Heerschap
  Department of Radiology, Radboud University Nijmegen Medical Center, Nijmegen, the Netherlands

c B. Weigelin, P. Friedl
  Department of Cell Biology, Nijmegen Center for Molecular Life Sciences, Radboud University Nijmegen Medical Center, Nijmegen, the Netherlands

† Present address: Grupo de Física Teórica, Instituto de Desarrollo Tecnológico para la Industria Química (CONICET-UNL) and Departamento de Materiales, FIQ-UNL, Santa Fe, Argentina

Abbreviations used: CE, perfluoro-[15]-crown-5 ether; DC, dendritic cell; PFC, perfluorocarbon; PLGA, poly(D,L-lactideco-glycolide).

The combined use of $^{19}F/^{1}H$ MR is a relatively new method employed to monitor ^{19}F-labeled cells quantitatively (20,24–26); a ^{19}F image can be obtained without any background (the detectable endogenous concentration of ^{19}F *in vivo* is negligible) for positive identification and quantification purposes, and a ^{1}H image is obtained separately for anatomic context. The approach has been described in detail elsewhere (27). ^{19}F MRI is well suited for quantitative cell tracking both *in vivo* and *in vitro*, as cell numbers can be quantified from the image data without the use of radioisotopes and the accompanying restriction on the length of time the cells remain detectable because of radioactive decay of the label. Moreover, recently, we have developed clinically applicable ^{19}F labels, consisting of polymer-encapsulated perfluorocarbon (PFC) particles (28). The use of particles, in place of the typical PFC emulsions, results in more stable and reproducible labeling of cells, which is necessary for accurate quantification.

In this article, we present a ^{19}F MR cell migration assay to track and quantify cell migration *in vitro* with spatial and time scales relevant to clinical and *in vivo* settings. Human DCs were embedded in gel scaffold layers specially designed to mimic living tissue (29–32). The porosity, stiffness and density were controlled to reproduce *in vivo* conditions with high fidelity. The density and volume of the cell layer were selected to reproduce typical cell bolus injection in patients. DC migration to an external gradient of chemokines was monitored and quantified, and the relationship between the cell density and migration rate was studied. Our study shows that the present ^{19}F MRI-based migration assay can be used as a complementary tool to typical light or fluorescence microscopy-based three-dimensional collagen single-cell migration methods (33–35) to evaluate the motion of cell populations on a realistic size scale. This assay also offers the possibility of direct translation to thick opaque samples, such as real tissues or *in vivo* conditions. Finally, we describe two different methods to quantify cell migration over time using our assay. The cell migration rates obtained here are comparable with patient data (36), thus validating our novel assay. Our data suggest a strong dependence of the migration rate on the initial cell density.

METHODS

^{19}F label

Particles with entrapped perfluoro-[15]-crown-5 ether (CE) ($C_{10}F_{20}O_5$) (Exfluor Research Corp., Round Rock, TX, USA) were prepared using poly(D,L-lactideco-glycolide) (PLGA; Resomer RG 502 H, lactide : glycolide molar ratio 48 : 52 to 52 : 48; Boehringer Ingelheim, Ingelheim am Rhein, Germany) as described (28). The particles contain 220 µg CE per milligram of PLGA, with an average diameter of 318 nm (28). The CE molecule contains 20 NMR-equivalent ^{19}F atoms, resulting in a single resonance peak.

Cell culture and labeling

DCs were generated from adherent peripheral blood mononuclear cells from donor blood by culturing in the presence of interleukin-4 (500 U/mL) and granulocyte–monocyte colony-stimulating factor (800 U/mL) (both Cellgenix, Freiburg, Germany), as described previously (37). Cells were cultured in X-VIVO-15 medium (BioWhittaker, Walkersville, MD, USA) with 2% human serum (Bloodbank; Rivierenland, Nijmegen, the Netherlands). A previously optimized dose (10 mg per 10^6 cells)

of PLGA–CE particles was added at day 3 (28). At day 6, the cells were matured by the addition of 10 µg/mL prostaglandin E$_2$ (Pharmacia & Upjohn, Puurs, Belgium), 10 ng/mL tumor necrosis factor-α, 5 ng/mL interleukin-1β and 15 ng/mL interleukin-6 (Cellgenix). On day 8, the cells were harvested using cold phosphate-buffered saline, and then washed three times in phosphate-buffered saline to remove excess particles. Cell viability was determined by trypan blue exclusion.

Scaffold migration assay

A three-dimensional collagen matrix was used as an interstitial support network to study DC migration. In brief, buffered collagen solution, adjusted with sodium bicarbonate (Invitrogen, Breda, the Netherlands) to pH 7.4, containing 1.67 µg/mL collagen (PureCol®, Advanced Biomatrix, San Diego, CA, USA) in X-VIVO-15 medium enriched with minimum essential Eagle's medium (Sigma-Aldrich, St. Louis, MO, USA), was homogeneously mixed and allowed to polymerize for 20–30 min at 37 °C (29,32).

The migration assay for ^{19}F tracking by MR (Fig. 1a) was based on three defined regions (from bottom to top): (i) the control region; (ii) the cell layer; and (iii) the migration region. The bottom layer (i) in all samples consists of a layer of gel (volume, 450 µL) to present a flat surface and to study any migration downwards caused by gravity or random migration; no chemokine was added. The next layer (ii) is the cell layer. This consists of the stated number of DCs (0.5–15 million) embedded in a fixed volume of 450 µL of gel scaffold. Directly above the cell layer, an external chemokine gradient was created in order to induce cell migration. A scaffold layer (iii) and X-VIVO-15 medium on top of it (both with a fixed volume of 450 µL) were set above the cell layer. This set-up results in a scaffold with a cylindrical shape of approximately 3 cm in length and 1 cm in diameter.

The chemokine gradient was established by adding different chemokine concentrations to both layers; 9 and 18 µL of recombinant human CCL21 (R&D Systems, Minneapolis, MN, USA) solutions in phosphate-buffered saline (10 µg/mL) were added to the scaffold and medium layers, respectively. The final chemokine concentrations used were optimized via bright-field, time-lapse microscopy to induce the maximum migration rates/speed on DCs in scaffolds.

The sample was placed upright in the MR magnet as soon as it was ready in order to avoid any potential migration caused by sample movement or gravity. The sample was then maintained in this position for the entire duration of the imaging experiment. All experiments were performed in triplicate.

Microscopy: speed and locomotion calculation

DCs were incorporated into a three-dimensional collagen matrix (PureCol®; final concentration, 1.7 mg/mL; 5×10^6 cells/mL) and overlaid with a cell-free second scaffold matrix layer which contained CCL21 (R&D Systems) at a low concentration (0.5 µg/mL) (Fig. 1b). To establish a steeper chemokine gradient, medium containing a high concentration of chemokine (CCL21, 1 µg/mL) was added adjacent to the cell-free collagen compartment.

DC migration into the cell-free collagen layer was recorded by digital time-lapse microscopy at a 2-min frame interval for up to 12 h. Computer-assisted cell tracking of randomly selected cells was performed as described previously (38).
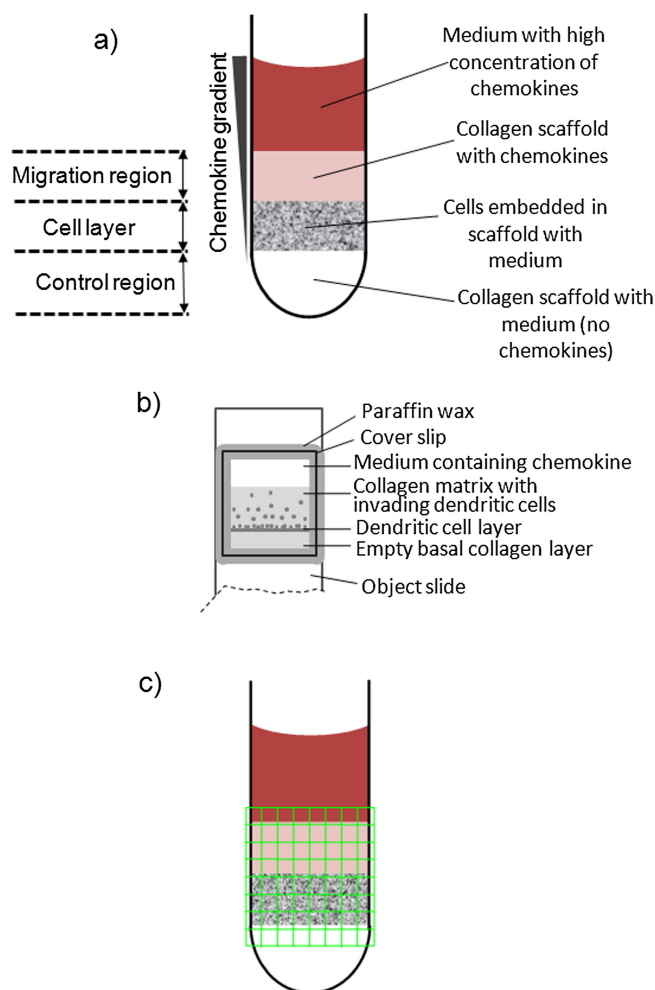
Figure 1. Experimental set-up. (a) Schematic view of the scaffold-based assay used to track dendritic cell (DC) migration with ¹⁹F MRSI. This assay design allows performance of the migration and control experiments simultaneously. (b) Migration chamber set-up for microscopy. Chambers were positioned upright and overlaid with CCL21 to monitor DC migration into the cell-free collagen layer by bright-field, time-lapse microscopy. (c) Frontal view of the chemical shift imaging grid used to study DC migration. As only the upward direction was considered to be relevant, the slice thickness was selected to cover the whole sample.

The time of active cell migration was calculated as the percentage of frames in which the cell moved by more than 1 μm/per frame (locomotion). The migration speed was calculated as the average step length/min within the complete observation time. The data from populations of 60 cells (two independent experiments) were combined. Statistical analysis was performed using a two-tailed Student's t-test for independent experiments.

MRSI

MRSI experiments were performed on a 7-T horizontal bore MR system (Clinscan, Bruker Biospin, Ettlingen, Germany), equipped with a horizontal bore magnet (ultra-shielded) and a gradient system with an inner diameter of 20 cm and maximum gradient strength of 300 mT/m. A 15-mm-diameter, 30-mm-long ¹H/¹⁹F bird cage/solenoid home-built body coil pair was used for the experiments.

A ¹⁹F MRSI sequence with elliptical k-space sampling was applied to track and quantify cell migration. This sequence consisted of a slice-selective pulse in a given direction, followed by phase encoding in the two other perpendicular directions. As we were interested only in the upward direction, projection

matrices were applied with 1.3×1-mm² in-plane resolution and a slice thickness of 10 mm (see Fig. 1c), with TR/TE = 600/2 ms, number of averages of 500 (total acquisition time, 61 min) and matrix size of 8×16. For localization, ¹H images were taken with the same resolution as the MRS images. The T_1 and T_2 values for the ¹⁹F spins in the fluorinated label were 950 ± 30 ms and 50 ± 8 ms, respectively, at 7 T. ¹⁹F T_1 was checked not to change between the initial and final time points of each experiment. ¹⁹F T_1 and T_2 were determined using well-known inversion recovery and Carr–Purcell–Meiboom–Gill sequences, respectively. No significant changes to these values were observed when the compound was internalized into the cells. MRS was used to determine the ¹⁹F content per cell with a calibrated reference of trifluoroacetic acid by applying an adiabatic 90° pulse to excite the whole sample. The number of ¹⁹F atoms was measured to be $(0.7 \pm 0.1) \times 10^{13}$ atoms/cell. The error value is the standard deviation of the fluorine content per cell obtained in seven independent samples.

The longitudinal tracking study of cell migration was accomplished by performing nine sequential experiments (nine time points) whilst maintaining the temperature of the sample at 37 °C for the entire duration of the experiment.

MRSI-based quantification

The ^{19}F MR spectrum corresponding to every voxel in the MRS image was collected and the intensity (area) of the peak corresponding to CE was determined (Syngo MR VB15 software, Siemens, Erlangen, Germany). The total intensity I_T (sum of all signal intensities from all voxels) was associated with the known total cell number N_T initially embedded in the gel scaffold. Finally, the number of cells N_v in a particular voxel v is given by:

$$N_v = \frac{I_v N_T}{I_T}$$

where I_v is the intensity corresponding to the voxel v.

MRI migration assessment

Two methods were used to evaluate cell migration.

Migration/control regions method

By the arbitrary definition of the regions immediately above (migration) and below (control) the initial cell layer, the cell number present in these regions was tracked over time. A comparison between trends in both regions was made to assess whether migration caused by the chemokine gradient was effectively produced. Migration rates were determined by contrasting cell numbers in the migration region for initial and final time points. This method tends to underestimate migration rates, as migration in the central region of the original cell layer is not taken into account.

Center of mass analysis

The vertical coordinate of the center of mass of the whole cell layer was tracked over time. From the trend of these curves, upward migration was assessed. All cells present in the cell layer were considered and subjective migration/control regions were not required. However, migration rates can only be obtained by estimating the average distance traveled by the cells.

RESULTS

^{19}F-labeling does not affect speed and locomotion (optical microscopy)

In order to study any effect of the label on cell migration, ^{19}F-PLGA-labeled and unlabeled cells were tested in the three-dimensional collagen matrix assay (38) and monitored by bright-field, time-lapse microscopy for migration efficiency (Fig. 2). The number of cells migrating out of the cell layer was equal in untreated control and PLGA-loaded DCs (Fig. 2a). Consistently, single-cell tracking of unlabeled and labeled cells showed that neither the average speed ($3 \pm 1\,\mu m/min$) nor the time periods over which DCs were actively migrating (Fig. 2b) were altered by PLGA loading. As a net result, DCs reached a median total distance of 1.8 mm in a 10-h observation time. Thus, the migration of DCs was not affected by ^{19}F-PLGA loading.

MRSI

As a proof of principle, the horizontal and vertical spatial cell number dependences in a given cell layer were calculated (Fig. 3). A semicircular-like profile was obtained for the horizontal
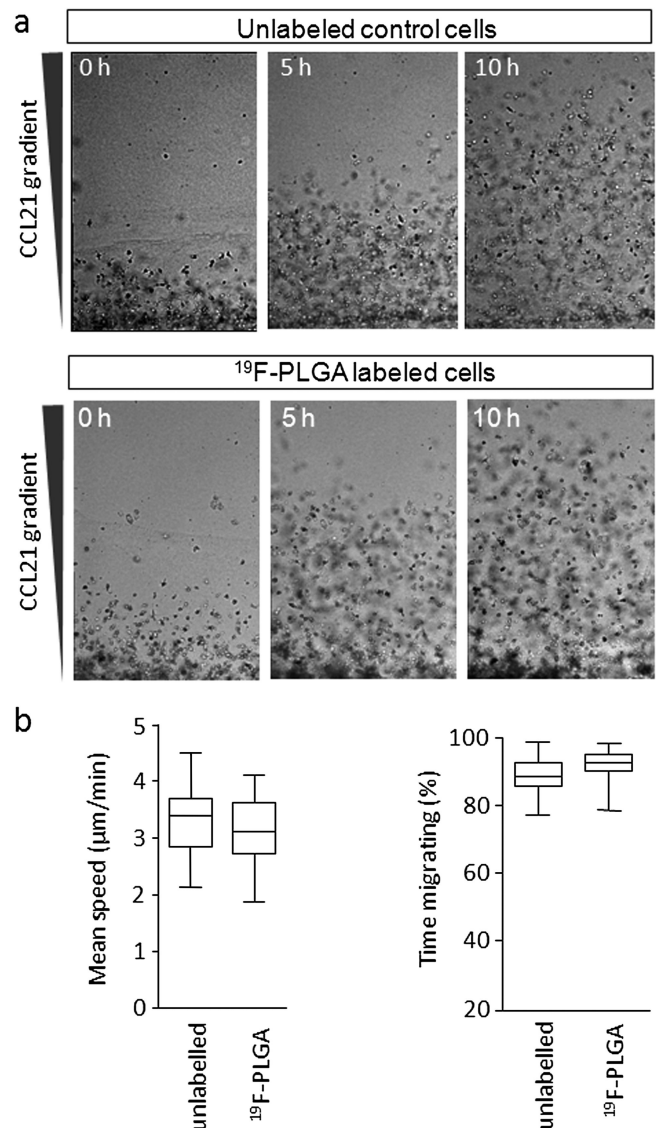
Figure 2. Microscopy showed no difference in migration on labeling. (a) Images of different time points for unlabeled and labeled cells showing migration towards the chemokine gradient region (upward direction). (b) Average speed and locomotion (percentage of time the cells were actively migrating) were quantified from populations of 60 cells (two independent pooled experiments). PLGA, poly(D,L-lactideco-glycolide). Statistical analysis was performed using a two-tailed Student's *t*-test for at least three independent experiments.

cell number profile. This result is a clear consequence of the projection of a cylindrical sample over a plane, as the slice thickness used in the MRSI sequence applied comprised the whole sample. In contrast, a more rectangular profile was obtained for the analogous vertical dependence, consistent with the expected shape of a cell layer. These profile plots provide clear signs of the reliability and consistency of the quantification method applied.

MRSI migration results are shown in Fig. 4. Initial and final five times interpolated cell layer maps are shown with the respective color chart for 15×10^6 (Fig. 4a), 10×10^6 (Fig. 4b), 5×10^6 (Fig. 4c), 1×10^6 (Fig. 4d) and 0.5×10^6 (Fig. 4e) cell layers. At first sight, slight migration can be observed in the top left part of Fig. 4c (5×10^6 cells) and mainly in the top right and left regions
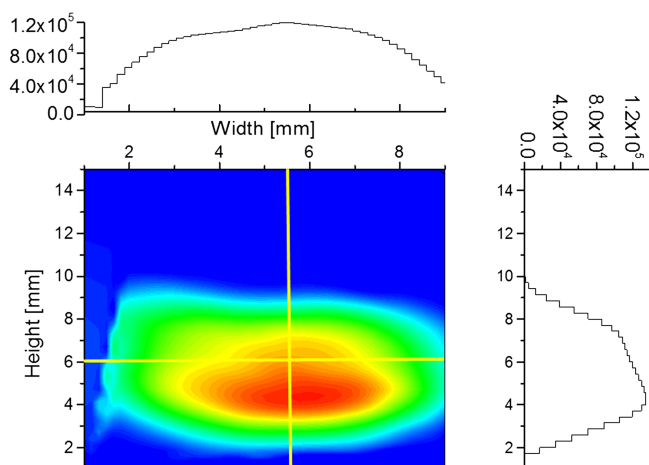
Figure 3. Proof of principle of the method. Cell layer profile for $N = 5 \times 10^6$ cells. The top graph plots the interpolated cell number as a function of the x position through the horizontal yellow line. A typical circular plot corresponding to the cylindrical shape of the Eppendorf tube is obtained. The cell number dependence in the y direction (relevant direction) for the vertical yellow line is shown in the right plot. A rectangular profile is obtained consistent with the expected shape of the layer.

of Fig. 4d (1×10^6 cells), and strong and clear upward migration is observed in the central region of Fig. 4e (0.5×10^6 cells). No apparent migration is observed in Fig. 4a and 4b, i.e. the higher cell numbers. Finally, no cells moved into the lower level, indicating that the movement in the upper level was caused by active migration.

It should be noted that all data analyses were performed on raw images or signal, although Figs 3 and 4 show interpolated images for easier visualization.

Migration assessment

Figure 4 (right) shows the evolution of the cell number in the migration (red) and control (blue) regions for 15×10^6, 10×10^6, 5×10^6, 1×10^6 and 0.5×10^6 cell layers. 'Migration' and 'control' regions are arbitrarily defined as zones immediately above and below the cell layer. These regions are plotted with broken yellow lines in Fig. 4a–e. It should be noted that chemokine-directed migration must occur in an upward direction, i.e. against gravity, in our set-up (Fig. 1).

For 15×10^6 cells, a variable trend was found in both the migration and control layers, without conclusive migration towards the chemokine gradient. With 10×10^6 cells, a variable trend was observed for the migration region, with a tendency to increase the cell number with time in the control region. Again, this indicates that no cell migration to the chemokine gradient region occurred. With 5×10^6 cells, the number of cells in the migration region increased over time, whereas a variable pattern was observed for the control region. This behavior clearly indicates upward migration to the chemokine gradient region. For the 1×10^6 cell layer, the observed trend for the migration region was even more pronounced than that of the 5×10^6 cell layer and, similarly, a nonsteady trend was observed for the control region. Here, upward migration is even more clearly demonstrated. For the 0.5×10^6 cell layer, upward migration was again clearly observed in the migration region but, also, a steady trend associated with random migration was clearly

observed in the control region. It should be noted, however, that the former process was much more significant than the latter. Random migration was only detected in this (0.5×10^6) case.

In order to quantify the number of cells moving to the migration region, the difference between the final and initial cell numbers in the migration region was calculated. For the 0.5×10^6 cell layer, migrating cells in the migration and control regions were subtracted. The results of three independent experiments are shown in Fig. 5 as a percentage of the total initial number of cells in the whole layer. From this plot, it is clear that cell migration to the chemokine gradient region increases when the cell density decreases below approximately 10^4 cells/μL. A one-sample, two-tailed Student's t-test was applied in order to establish whether migration occurred: the p values obtained were 0.015, 0.0057, 0.0059, 0.42 and 1 for the 0.5×10^6, 1×10^6, 5×10^6, 10×10^6 and 15×10^6 cases. In the first three cases, the p values obtained (< 0.05) indicate a statistically significant migration. In the other two cases, the p values indicate no significant differences between the rates obtained and null migration.

Migration was also assessed by monitoring the evolution of the vertical coordinate of the center of mass of the cell layer (Fig. 6). Although erratic patterns were obtained for the 15×10^6 and 10×10^6 cell layers, the vertical position of the center of mass steadily increased with time for the 5×10^6, 1×10^6 and 0.5×10^6 cell layers. All graphs are shown with the same y-scale step (0.01 mm). Consistent with the previous method, a stronger increase in the center of mass position was observed for the 0.5×10^6 and 1×10^6 cell layers when compared with the 5×10^6 case. To prove our point, the same analysis was applied to the horizontal position of the center of mass and the corresponding evolutions are shown in the insets of Fig. 6. An erratic pattern was observed in all of them and the maximum shift in the horizontal position of the center of mass was 0.02 mm. This result was used to calculate the p values of a one-sample Student's t-test. The p values obtained (where the hypothetical mean was taken as 0.02 mm) were 0.41, 0.35, 0.045, 0.015 and 0.01 for the 15×10^6, 10×10^6, 5×10^6, 1×10^6 and 0.5×10^6 cell layers, respectively. It should also be noted that the general trends observed in the main plots of Figs. 6 and cell numbers in the migration region (red charts in Fig. 5) are similar, showing the consistency between the two methods.

DISCUSSION

We have developed and applied a novel cell migration assay using ¹⁹F MRI to monitor DC migration to optimize DC vaccine delivery to patients. The microscopy results showed that labeling does not affect the speed or locomotion of labeled cells (Fig. 1). Previously, cell viability has been shown to be unchanged after loading 0.7×10^{13} ¹⁹F atoms/cell (28). The sensitivity of this technique under these conditions was determined to be about 5000 cells per voxel for a 1-h measurement (signal-to-noise ratio, 3).

Cell migration in the MRSI assay was assessed by two independent methods, both of which showed that cells migrated upwards because of the chemokine. The migration/control regions method has the disadvantage that only migration in the region above or below the cell layer was considered. This method tends to underestimate migration rates as any potential migration in the central part of the cell layer is disregarded.

The center of mass method accounts for migration anywhere in the sample, but quantitative migration cell rates are difficult
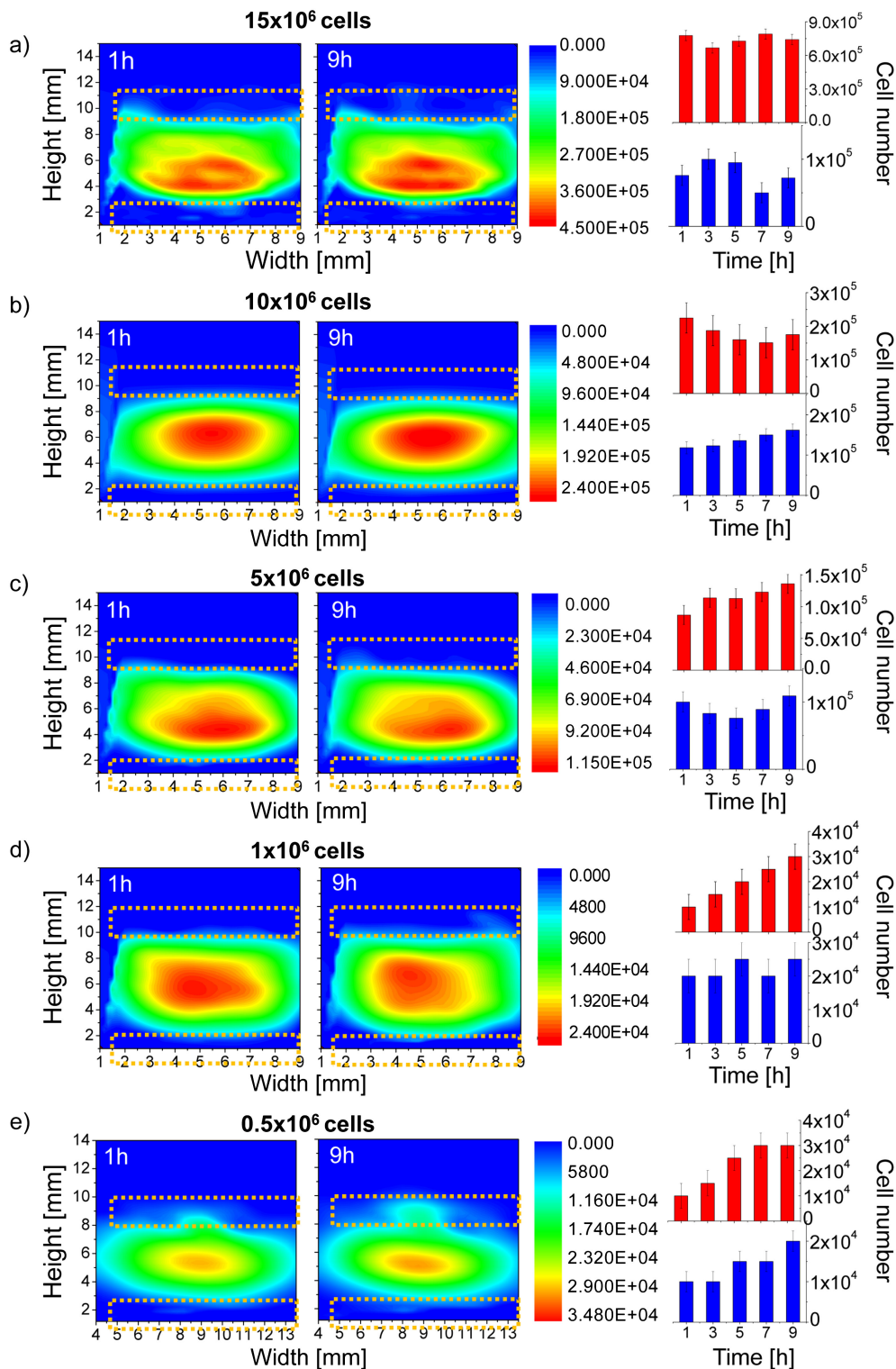
Figure 4. MRSI results – migration assessment. Initial (1 h) and final (9 h) cell maps obtained with ^{19}F MRSI for 15×10^6 (a), 10×10^6 (b), 5×10^6 (c), 1×10^6 (d) and 0.5×10^6 (e) dendritic cells (DCs) embedded in three-dimensional collagen scaffolds. The migration and control selected regions are indicated by broken yellow line boxes. The color chart indicates the cell number associated with a given color. The corresponding changes in cell number within the migration and control regions are plotted as red and blue bar charts, respectively (right). A clear trend is observed for the cell number time dependence in the migration region for 5×10^6, 1×10^6 and 0.5×10^6 cell layers. No pattern is observed for higher cell numbers.

to extract. Two main factors can be responsible for a shift in the center of mass position: the number of migrating cells and the average distance traveled. As cells cannot be tracked individually (sensitivity issues), the average distance cannot be determined,

and the migrating cell number can only be calculated approximately by estimating the average distance traveled. For instance, for the 1×10^6 experiment, if the average distance traveled is roughly assumed to be 1 mm in 10 h, the observed 0.08-mm shift
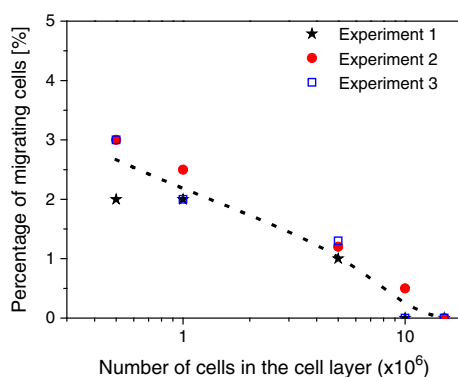
Figure 5. Migration rates. Difference between final (9 h) and initial (1 h) cell numbers in the migration region. The numbers are plotted as a percentage of the total number of cells inserted. Results from three independent experiments are plotted. The dotted line represents the general trend observed.

in the center of mass position translates to a migration rate of 8%. This value is higher, but in the same order of magnitude, as the value obtained with the previous method. It is important to remark that the previous calculation does not include potential counter-effects by cells migrating in the downward direction.

Another remarkable observation is that no cells were found further than 2 mm from their original location. This result is consistent with the average speed determined using microscopy as, according to this result, cells travel, on average, 1.8 mm. Although cells travel to a preferred direction in the x–y plane (vertically), horizontal motion certainly occurs. Therefore, no cells are expected to be found at a distance greater than 1.8 mm from the borders of the initial cell layer for the time window studied. It

should be noted that we were only interested in migration along the chemokine gradient, and thus the voxels have higher resolution in the vertical plane. Higher resolution or three-dimensional imaging can be used to study migration in the horizontal plane. The main limitation of the method is the signal-to-noise ratio achieved by the image acquisition technique, as discussed in a review on ¹⁹F MRI for cell tracking (30). With our imaging conditions, we could detect down to 5000 cells per voxel per hour of imaging time. We chose to measure the samples every hour, but, in principle, fewer time points are necessary, and thus longer acquisitions are possible to enhance the signal-to-noise ratio. Given the typical distances traveled by cells in the time scale of the total experiment (~ 10 h), the voxel size (spatial resolution) was selected to have the maximum volume (to maximize the signal-to-noise ratio) for the minimum necessary size to detect migration during the experiment. A lower spatial resolution could be used if detailed information on cell motion is required, provided that migration rates are sufficiently high to allow cell detection.

Any partial volume effect typically occurring in MRSI acquisition was neglected in the present quantification method. Although partial volume effects might become important when detecting small signals, they have no influence on the final results as all the results are referred to the zero time point experiment, thus removing any potential influence on the migration ratios. Moreover, this effect might cause a slight underestimation of the minimum detectable cell number (overestimation of the sensitivity) because of the method used to calculate the number of cells from the total signal (see Methods).

We also found that free PLGA–Perfluoro–15–crown–5–ether particles do not diffuse in the collagen matrix over the time period of the experiment. This was tested using free label in place of labeled cells in a similar migration set-up (data not shown). Thus, any leaked label
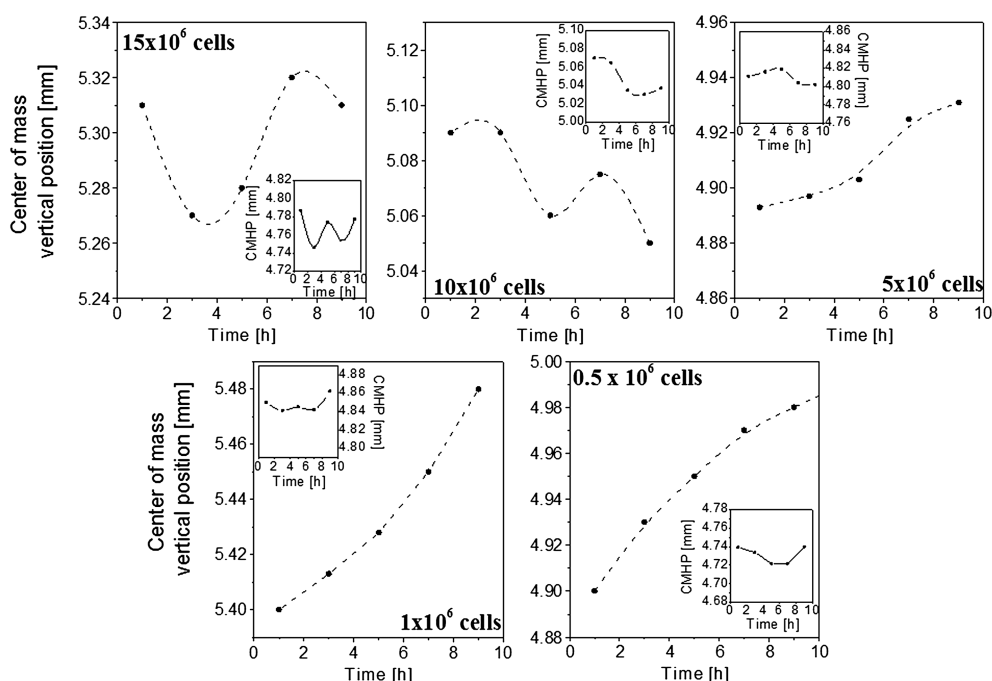
Figure 6. Migration assessment with center of mass analysis. The vertical position of the center of mass is plotted as a function of time for different cell layer densities. An erratic pattern is observed for the evolution of the center of mass horizontal position (CMHP) (insets). A clear trend indicating upward migration is observed for 5×10^6, 1×10^6 and 0.5×10^6 cell layers.

from dead or dying cells would be stationary and not be reflected as migration in our assay. Moreover, the ^{19}F content per cell is known to be homogeneous with PLGA–Perfluoro–15–crown–5–ether (28).

The cell migration rates obtained in this study showed a strong dependence on the initial cell layer density. Migration rates increased with decreasing cell density. A possible explanation for this behavior is that cells suffer from overcrowding conditions: a lack of oxygen and nutrients may cause cell death or loss of migratory capabilities. It should be noted that our migration gels were incubated in humidified, sterile conditions in the presence of culture medium to ensure good oxygenation throughout the sample at the start of the experiment. Furthermore, the temperature was maintained throughout the experiment. We also found that the T_1 of PFC did not change over the course of the experiment, although some PFCs are known to be oxygen sensitive (9,39). CE encapsulation by polymeric PLGA particles is probably responsible for the apparent insensitivity of the fluorinated compound T_1 to the oxygen partial pressure. Nevertheless, PLGA encapsulation is necessary as the CE is otherwise insoluble and therefore not available for cell uptake.

We observed a 'saturation behavior' for the migration rate *versus* cell layer density curve, once the optimum density conditions had been reached. Assuming spherical cells, an average diameter of $25\,\mu m$ for each labeled cell translates to a total volume of about $122\,\mu L$ for 15×10^6 cells. Given that the total volume of the cell layer is $450\,\mu L$, this gives an average space per cell of about 3.75 times its own volume. This results in an average distance of about $39\,\mu m$ between adjacent cells. For 1×10^6 cells, this average distance increases to almost $100\,\mu m$ and the average space per cell becomes 15 times higher. To examine this conjecture, it is essential to monitor the viability of the cells under the same experimental conditions as in the MRI experiments. In addition, the optimum cell density for a specific application will vary depending on whether the total number of migratory cells or the percentage of the total cell number needs to be maximized.

In this article, we have presented a novel ^{19}F MR-based three-dimensional assay to study cell migration in a large-scale sample, comparable with the clinical situation. As MRI is not an optical technique, all the results obtained in the present work can be translated directly to opaque samples, giving the chance to assess cell migration *in vitro* under conditions very close to the *in vivo* situation. Unlike conventional assays for migration, such as microscopy or the Transwell assay (40), this assay can be applied to both larger numbers of cells and opaque samples. Here, we tested the effect of labeling itself on cell migration using a more conventional light microscopy assay for migration. However, we could not test the effect of different cell densities using the same technique, because of the total cell number limitation and the nonquantitative character of the technique. The ^{19}F-based migration assay presented here is not intended to replace optical assays, but is a complementary tool to these assays for cell migration analysis.

Furthermore, as certain PFCs are sensitive to oxygen partial pressure, the particles and measurement technique could also be adjusted to assess oxygen tension in different regions of the sample. This application could be very important if migration is influenced by the oxygen content and overcrowding effects. Moreover, here, we tested a single chemokine and a single CCL21 chemokine gradient (typical of migration assays) that are known to be directly involved in DC migration as a proof of principle, although the assay itself could be easily amended to test different chemokines, chemokine gradients or even combinations of chemokines. Finally, the same imaging and quantification technique could be adapted directly to *in vivo* applications, even in the clinic. Thus, the assay is highly suited to optimize the migration of clinical cellular therapy *in vitro* in a cost-effective and reproducible manner, without the logistic and technical difficulties associated with clinical imaging studies.

REFERENCES

1. Banchereau J, Steinman RM. Dendritic cells and the control of immunity. Nature 1998; 392: 245–252.
2. Reis e Sousa C. Dendritic cells in a mature age. Nat. Rev. Immunol. 2006; 6: 476–483.
3. Aarntzen EH, Figdor CG, Adema GJ, Punt CJ, de Vries IJ. Dendritic cell vaccination and immune monitoring. Cancer Immunol. Immunother. 2008; 57(10): 1559–1568.
4. Banchereau J, Palucka A. Dendritic cells as therapeutic vaccines against cancer. Nat. Rev. Immunol. 2005; 5: 296–306.
5. Lesterhuis WJ, de Vries IJ, Adema GJ, Punt CJ. Dendritic cell-based vaccines in cancer immunotherapy: an update on clinical and immunological results. Ann. Oncol. 2004; 15(Suppl. 4): iv145–iv151.
6. Steinman RM, Banchereau J. Taking dendritic cells into medicine. Nature 2007; 449(7161): 419–426.
7. De Vries IJ, Krooshoop DJ, Scharenborg NM, Lesterhuis WJ, Diepstra JH, Van Muijen GN, Strijk SP, Ruers TJ, Boerman OC, Oyen WJ, Adema GJ, Punt CJ, Figdor CG. Effective migration of antigen-pulsed dendritic cells to lymph nodes in melanoma patients is determined by their maturation state. Cancer Res. 2003; 63(1): 12–17.
8. de Vries IJ, Lesterhuis WJ, Barentsz JO, Verdijk P, van Krieken JH, Boerman OC, Oyen WJ, Bonenkamp JJ, Boezeman JB, Adema GJ, Bulte JW, Scheenen TW, Punt CJ, Heerschap A, Figdor CG. Magnetic resonance tracking of dendritic cells in melanoma patients for monitoring of cellular therapy. Nat. Biotechnol. 2005; 23(11): 1407–1413.
9. Srinivas M, Aarntzen EH, Bulte JW, Oyen WJ, Heerschap A, de Vries IJ, Figdor CG. Imaging of cellular therapies. Adv. Drug Deliv. Rev. 2010; 62(11): 1080–1093.
10. Figdor CG, de Vries IJ, Lesterhuis WJ, Melief CJ. Dendritic cell immunotherapy: mapping the way. Nat. Med. 2004; 10: 475–480.
11. Verdijk P, Aarntzen EH, Punt CJ, de Vries IJ, Figdor CG. Maximizing dendritic cell migration in cancer immunotherapy. Expert Opin. Biol. Ther. 2008; 8(7): 865–874.
12. Valster A, Tran NL, Nakada M, Berens ME, Chan AY, Symons M. Cell migration and invasion assays. Methods 2005; 37(2): 208–215.
13. Schimmelpfennig CH, Schulz S, Arber C, Baker J, Tarner I, McBride J, Contag CH, Negrin RS. Ex vivo expanded dendritic cells home to T-cell zones of lymphoid organs and survive in vivo after allogeneic bone marrow transplantation. Am. J. Pathol. 2005; 167: 1321–1331.
14. Olasz EB, Lang L, Seidel J, Green MV, Eckelman WC, Katz SI. Fluorine-18 labeled mouse bone marrow derived dendritic cells can be detected in vivo by high resolution projection imaging. J. Immunol. Methods 2002; 260: 137–148.
15. Prince HM, Wall DM, Ritchie D, Honemann D, Harrrison S, Quach H, Thompson M, Hicks R, Lau E, Davison J, Loudovaris M, Moloney J, Loveland B, Bartholeyns J, Katsifis A, Mileshkin L. In vivo tracking of dendritic cells in patients with multiple myeloma. J. Immunother. 2008; 31: 166–179.
16. Eggert AA, van der Voort R, Torensma R, Moulin V, Boerman OC, Oyen WJ, Punt CJ, Diepstra H, de Boer AJ, Figdor CG, Adema GJ.

Analysis of dendritic cell trafficking using EGFP-transgenic mice. Immunol. Lett. 2003; 89: 17–24.

17. Mackensen A, Krause T, Blum U, Uhrmeister P, Mertelsmann R, Lindemann A. Homing of intravenously and intralymphatically injected human dendritic cells generated in vitro from CD34+ hematopoietic progenitor cells. Cancer Immunol. Immun. 1999; 48: 118–122.

18. Noh Y, Lim YT, Chung BH. Noninvasive imaging of dendritic cell migration into lymph nodes using near-infrared fluorescent semiconductor nanocrystals. FASEB J. 2008; 22: 3908–3918.

19. Sen D, Deerinck TJ, Ellisman MH, Parker I, Cahalan MD. Quantum dots for tracking dendritic cells and priming an immune response in vitro and in vivo. PLoS One 2008; 3(9): e3290.

20. Ahrens ET, Flores R, Xu H, Morel PA. In vivo imaging platform for tracking immunotherapeutic cells. Nat. Biotechnol. 2005; 23(8): 983–987.

21. Baumjohann D, Hess A, Budinsky L, Brune K, Schuler G, Lutz MB. In vivo magnetic resonance imaging of dendritic cell migration into the draining lymph nodes of mice. Eur. J. Immunol. 2006; 36: 2544–2555.

22. Helfer BM, Melson AD, Janjic JM, Gil RR, Kalinski P, de Vries J, Ahrens ET, Mailliard RB. Functional assessment of human dendritic cells labeled for in vivo ^{19}F magnetic resonance imaging cell tracking. Application of a novel ^{19}F tracer agent for in vivo tracking of human dendritic cell vaccines. Cytotherapy 2010; 12: 238–250.

23. Verdijk P, Scheenen TW, Lesterhuis WJ, Gambarota G, Veltien AA, Walczak P, Scharenborg NM, Bulte JW, Punt CJ, Heerschap A, Figdor CG, de Vries IJ. Sensitivity of magnetic resonance imaging of dendritic cells for in vivo tracking of cellular cancer vaccines. Int. J. Cancer 2007; 120(5): 978–984.

24. Ruiz-Cabello J, Walczak P, Kedziorek DA, Chacko VP, Schmieder AH, Wickline SA, Lanza GM, Bulte JW. In vivo 'hot spot' MR imaging of neural stem cells using fluorinated nanoparticles. Magn. Reson. Med. 2008; 60(6): 1506–1511.

25. Srinivas M, Morel PA, Ernst LA, Laidlaw DH, Ahrens ET. Fluorine-19 MRI for visualization and quantification of cell migration in a diabetes model. Magn. Reson. Med. 2007; 58(4): 725–734.

26. Srinivas M, Turner MS, Janjic JM, Morel PA, Laidlaw DH, Ahrens ET. In vivo cytometry of antigen-specific T cells using (19)F MRI. Magn. Reson. Med. 2009; 62: 747–753.

27. Srinivas M, Heerschap A, Ahrens ET, Figdor CG, de Vries IJ. [19]F MRI for quantitative in vivo cell tracking. Trends Biotechnol. 2010; 28: 363–370.

28. Srinivas M, Cruz LJ, Bonetto F, Heerschap A, Figdor CG, de Vries IJ. Customizable, multi-functional fluorocarbon nanoparticles for quantitative in vivo imaging using ^{19}F MRI and optical imaging. Biomaterials 2010; 31: 7070–7077.

29. Friedl P, Brocker EB. The biology of cell locomotion within three-dimensional extracellular matrix. Cell. Mol. Life Sci. 2000; 57: 41–64.

30. Lauffenburger DA, Horwitz AF. Cell migration: a physically integrated molecular process. Cell 1996; 84: 359–369.

31. Petrie RJ, Doyle AD, Yamada KM. Random versus directionally persistent cell migration. Nat. Rev. Mol. Cell Biol. 2009; 10: 538–549.

32. Even-Ram S, Yamada KM. Cell migration in 3D matrix. Curr. Opin. Cell Biol. 2005; 17: 524–532.

33. Demou ZN, McIntire LV. Fully automated three-dimensional tracking of cancer cells in collagen gels: determination of motility phenotypes at the cellular level. Cancer Res. 2002; 62: 5301–5307.

34. Friedl P, Noble PB, Zanker KS. Lymphocyte locomotion in three-dimensional collagen gels. Comparison of three quantitative methods for analysing cell trajectories. J. Immunol. Methods 1993; 165: 157–165.

35. Niggemann B, Drell TL, Joseph J, Weidt C, Lang K, Zaenker KS, Entschladen F. Tumor cell locomotion: differential dynamics of spontaneous and induced migration in a 3D collagen matrix. Exp. Cell Res. 2004; 298: 178–187.

36. Verdijk P, Aarntzen EH, Lesterhuis WJ, Boullart AC, Kok E, van Rossum MM, Strijk S, Eijckeler F, Bonenkamp JJ, Jacobs JF, Blokx W, Vankrieken JH, Joosten I, Boerman OC, Oyen WJ, Adema G, Punt CJ, Figdor CG, de Vries IJ. Limited amounts of dendritic cells migrate into the T-cell area of lymph nodes but have high immune activating potential in melanoma patients. Clin. Cancer Res. 2009; 15(7): 2531–2540.

37. Boullart AC, Aarntzen EH, Verdijk P, Jacobs JF, Schuurhuis DH, Benitez-Ribas D, Schreibelt G, van de Rakt MW, Scharenborg NM, de Boer A, Kramer M, Figdor CG, Punt CJ, Adema GJ, de Vries IJ. Maturation of monocyte-derived dendritic cells with Toll-like receptor 3 and 7/8 ligands combined with prostaglandin E2 results in high interleukin-12 production and cell migration. Cancer Immunol. Immunother. 2008; 57(11): 1589–1597.

38. Friedl P, Brocker EB. Reconstructing leukocyte migration in 3D extracellular matrix by time-lapse videomicroscopy and computer-assisted tracking. In Methods in Molecular Biology, Vol. 239. D'Ambrosio D, Sinigaglia F (eds). Humana Press: New York; 2003, pp. 77–90.

39. Kadayakkara D, Janjic J, Pusateri L, Young W-B, Ahrens ET. In vivo observation of intracellular oximetry in perfluorocarbon-labeled glioma cells and chemotherapeutic response in the CNS using fluorine-19 MRI. Magn. Reson. Med. 2010; 64: 1252–1259.

40. Decaestecker C, Debeir O, Van Ham P, Kiss R. Can anti-migratory drugs be screened in vitro? A review of 2D and 3D assays for the quantitativeanalysis of cell migration. Med. Res. Rev. 2007; 27: 149–176.

Research Article

A large-scale ^{19}F MRI-based cell migration assay to optimize cell therapy

F. Bonetto, M. Srinivas, B. Weigelin, L. J. Cruz, A. Heerschap, P. Friedl, C. G. Figdor and I. J. M. de Vries
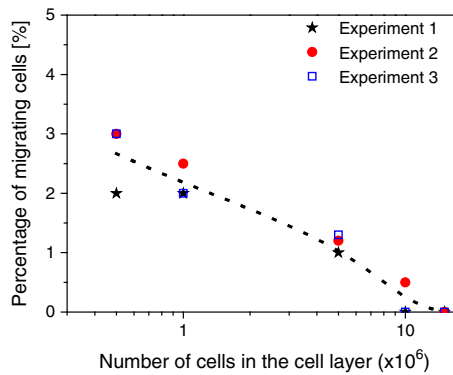
A novel ^{19}F MR-based, large-scale quantitative assay to measure cell migration in three-dimensional opaque samples is introduced. Migration rates in the present assay were assessed for different cell densities of ^{19}F-labeled human dendritic cells using two different methods. No migration was found for high cell densities, and up to 3% was found for low cell densities. Consequently, we show that cell density has a decisive impact on migration in cell bolus injections.